

# Spatial–temporal evolution of photospheric weak-field shifts in solar cycles 21–24

K. Mursula, T. Getachew, and I. I. Virtanen

Space Climate Research Group, Space Physics and Astronomy Research Unit, University of Oulu, PO Box 3000, 90014 Oulu, Finland  
e-mail: kalevi.mursula@oulu.fi

Received 14 October 2019 / Accepted 6 October 2020

## ABSTRACT

**Context.** Weak magnetic field elements make a dominant contribution to the total magnetic field on the solar surface. Even so, little is known of their long-term occurrence.

**Aims.** We study the long-term spatial–temporal evolution of the weak-field shift and skewness of the distribution of photospheric magnetic field values during solar cycles 21–24 in order to clarify the role and relation of the weak field values to the overall magnetic field evolution.

**Methods.** We used Wilcox Solar Observatory (WSO) and the Synoptic Optical Long-term Investigations of the Sun Vector SpectroMagnetograph synoptic maps to calculate weak-field shifts for each latitude bin of each synoptic map, and thereby constructed a time–latitude butterfly diagram for shifts. We also calculated butterfly diagrams for skewness for all field values and for weak field values only.

**Results.** The weak-field shifts and (full-field) skewness depict a similar spatial–temporal solar cycle evolution to that of the large-scale surface magnetic field. The field distribution has a systematic non-zero weak-field shift and a large skewness already at (and after) the emergence of the active region, even at the highest resolution. We find evidence for coalescence of opposite-polarity fields during the surge evolution. This is clearly more effective at the supergranulation scale. However, a similar dependence of magnetic field coalescence on spatial resolution was not found in the unipolar regions around the poles.

**Conclusions.** Our results give evidence for the preference of even the weakest field elements toward the prevailing magnetic polarity since the emergence of an active region, and for a systematic coalescence of stronger magnetic fields of opposite polarities to produce weak fields during surge evolution and at the poles. We also find that the supergranulation process is reduced or turned off in the unipolar regions around the poles. These observations improve the understanding not only of the development of the weakest magnetic field elements, but also of the dynamics of magnetic fields at large, and even of processes below the solar surface.

**Key words.** Sun: magnetic fields

## 1. Introduction

Sunspots and other active regions are the most intense manifestations of solar magnetic fields emerging on the solar surface. Produced by the solar dynamo mechanism, their occurrence waxes and wanes during the well-known sunspot cycle of roughly 11 years. Both the large-scale solar magnetic field and the polarity order of a bipolar sunspot pair change from one cycle to the next, leading to a 22-year solar magnetic cycle (the Hale cycle) consisting of two sunspot activity cycles (for historical reviews, see, e.g., [van Driel-Gesztelyi & Green 2015](#); [Stenflo 2017](#)).

The large-scale magnetic field of the solar photospheric surface is mainly formed by the emergence and subsequent evolution (e.g., diffusion, transport) of active regions. Most bipolar active regions follow Joy’s law ([Hagenaar et al. 2003, 2008](#); [Tlatov et al. 2010](#); [van Driel-Gesztelyi & Green 2015](#)), according to which the axis of the bipole is tilted with respect to the east–west direction ([Hale et al. 1919](#)). The trailing parts of active regions are at a somewhat higher latitude and form poleward-moving new-polarity surges, which eventually cancel the old-polarity field of the pole during sunspot maxima and create there a magnetic field with polarity opposite to that of the previous solar minimum ([Babcock 1961](#); [Leighton 1969](#)).

The photospheric magnetic field is rather complex and includes a wide range of large-scale and small-scale structures.

While the strongest magnetic fields are found in active regions containing sunspots ([Okamoto & Sakurai 2018](#)), small-scale structures with magnetic fields that are several (six to seven) orders of magnitude weaker have been measured. Due to an increasing spatial and spectral resolution of magnetic field measurements, the magnetism of the quiet Sun (the solar surface outside active regions) and the smallest and weakest magnetic features have become a topic of active research (see the review by [Stenflo 1989](#) and papers by, e.g., [Lites 2002](#); [Berger & Lites 2002, 2003](#); [Stenflo 2010, 2014](#)).

The photospheric magnetic field consists mainly of rather weak fields, irrespective of spatial accuracy. Although the typical flux of an active region is about two orders of magnitude higher than that of an ephemeral region, the greater emergence rate (about  $10^4$  times) of ephemeral regions makes their total flux exceed that of active regions by two orders of magnitude ([Zirin 1987](#)). Similarly, even the smaller scale fields (e.g., network and internetwork) produce more total flux to the surface than the ephemeral regions. Accordingly, the contribution of weak small-scale fields to the total flux on the solar surface is dominant. This makes the better understanding of weak small-scale magnetic fields acutely important.

Only relatively few studies have concentrated on the large-scale properties of the weakest photospheric magnetic field values. Some early studies on weak magnetic fields have found

evidence of an asymmetric polarity distribution of weak fields (Ulrich et al. 2002; Berger & Lites 2002; Liu et al. 2004). However, while some of these studies considered this asymmetry to be a real physical feature of the weak fields (Liu et al. 2004), others suggested that it is a random pattern related to the artifact of measurement noise (Ulrich et al. 2002). This left the evidence of an asymmetric polarity distribution of weak fields inconclusive.

We have recently revisited this question and studied the statistical significance (Getachew et al. 2019a) and the temporal evolution (Getachew et al. 2019b) of weak photospheric magnetic fields in great detail. Our results have given conclusive evidence of a systematically asymmetric distribution of weak fields. We showed that several independent magnetograph instruments and different synoptic map datasets with different resolutions gave same-signed, statistically significant weak-field asymmetries for the same solar rotations, and that these asymmetries depicted similar systematic temporal variations (Getachew et al. 2019a). The weak-field asymmetry was found to increase when the spatial resolution of the synoptic map was reduced, with the largest increase found when approaching the spatial scale of solar supergranulation. We also showed that the asymmetries calculated for the two hemispheres separately always have the same sign as the new polarity of the polar field in the respective hemisphere and solar cycle, and attain their maximum in the early to mid-declining phase of the solar cycle. These results strongly suggest that the weak-field asymmetries are an important element of solar magnetism.

In this paper we study the latitudinal distribution of weak field values and the related weak-field asymmetry (shift) and their hemispheric means using the high-resolution data from the Synoptic Optical Long-term Investigations of the Sun (SOLIS) Vector SpectroMagnetograph (VSM), and the low-resolution data from the Wilcox Solar Observatory. The paper is organised as follows. Section 2 presents the data and methods used in this study. Section 3 studies the long-term evolution of weak-field shifts in Wilcox Solar Observatory (WSO) data using a weak-field shift butterfly diagram. Section 4 shows the shift butterfly for SOLIS/VSM data and discusses the effect of spatial resolution to the observed evolution of hemispheric shifts. Section 5 presents the SOLIS butterfly diagram of skewness using both all field values and only weak-field values, and discusses their difference and relation to the observed weak-field shift distribution. Finally, we discuss the results in Sect. 6 and give our conclusions in Sect. 7.

## 2. Data and methods

We use synoptic maps of the photospheric pseudo-radial magnetic field measured at WSO and SOLIS/VSM. WSO synoptic maps have a fairly low spatial resolution of only  $72 \times 30$  pixels in longitude and sine-latitude, with the highest latitude bin centered at  $\pm 75.2^\circ$ . However, the virtue of WSO measurements is that the same instrumentation has been in operation since the measurements started. WSO synoptic maps present the line-of-sight field, of which we calculated the pseudo-radial field. (Details about the WSO magnetograph, data calibration, and reduction methods can be found in, e.g., Hoeksema 1984). We used 569 synoptic maps (F-data maps with missing data filled by interpolation) from CR 1642 to CR 2210 (i.e., 1976.3–2018.8). We found earlier that in 1996–1999 and in 2001.1–2001.5 the WSO data are erroneous and in clear disagreement with other datasets; see, e.g., Virtanen & Mursula (2016, 2017). We leave this period of erroneous data out of the subsequent analysis.

The SOLIS/VSM instrument of the National Solar Observatory (NSO) produced high-resolution synoptic maps of the

pseudo-radial magnetic field (with no polar filling) from CR 2007 to CR 2196 (i.e., 2003.7–2017.8). (For details on SOLIS/VSM data, see, e.g., Bertello et al. 2014.) In this work we use the SOLIS/VSM synoptic maps given at  $1800 \times 900$  pixel resolution (equally spaced in longitude and sine-latitude). Furthermore, using these maps, we calculated four sets of lower resolution synoptic maps ( $360 \times 180$ ,  $180 \times 75$ ,  $120 \times 50$ , and  $72 \times 30$ ) by simple block-averaging (for more details, see Getachew et al. 2019a).

We define the weak-field shift in the same way as earlier (Getachew et al. 2019a,b), as the location of the maximum of the Gaussian fit to the histogram distribution of weak-field values between  $-10$  G and  $+10$  G. We note that the shifts are practically independent of the range of weak field values, as noted in Getachew et al. (2019a) (see also Liu et al. 2004). In addition to the hemispheric means of weak-field shifts of each synoptic map, already discussed in Getachew et al. (2019b), we now also calculate the shift for each latitude bin of each synoptic map. This allows us to construct a similar time-latitude diagram for shifts that is often used to demonstrate the temporal evolution of the longitudinally averaged magnetic field (also called the magnetic butterfly diagram or the super-synoptic map).

## 3. WSO butterflies

The upper panel of Fig. 1 shows the shift butterfly diagram, i.e., the weak-field shift values for each latitude bin and each WSO synoptic map. The middle panel depicts the hemispheric (north and south) shifts for each rotation for the same dataset (same as in Fig. 3 of Getachew et al. 2019b). The bottom panel of Fig. 1 presents the normal butterfly diagram, i.e., the longitudinally averaged magnetic field for each latitude bin and rotation.

It is mesmerizing how closely the shift butterfly diagram resembles the normal butterfly diagram. Both diagrams demonstrate the basic facts of the cyclic evolution of the solar surface magnetic fields: the appearance of new flux at low to mid-latitudes around sunspot maximum times, the subsequent development of poleward surges of (mainly) trailing polarity flux, which eventually then turn the magnetic polarity of the solar poles. The sign (polarity) of the weak-field shift is the same as the polarity of the large-scale field for each surge and for the poles. Sometimes the individual surges can be seen even slightly better in the shift butterfly diagram than in the normal butterfly diagram. This is the case, for example, in the southern hemisphere in the late 1970s and early 2000s, and in the north around 1990.

We have included vertical lines in Fig. 1 in order to delineate the timing of the main extrema of the hemispheric shifts depicted in the middle panel. Following these vertical lines into the two butterfly diagrams, we can see in which surges and at which phase of the solar cycle these extrema of the hemispheric shifts occur. Starting from the two noted (negative) extrema of the northern shift in 1980 and 1982 (soon after the maximum of solar cycle 21), the upper panel of Fig. 1 shows that both of these times correspond to a situation when a negative-shift surge has reached the pole and negative shift values extend over a very wide latitude range from mid-latitudes to the pole. The lower panel of Fig. 1 shows a very similar situation for the magnetic field. Both of the two shift extrema occur at times when a negative-polarity surge, which earlier started drifting poleward, has reached the pole. The first surge, corresponding to the shift extremum in 1980, has just turned the polarity of the pole, while the second surge, corresponding to the shift extremum in 1982, intensifies the pre-existing new polarity of the pole. The

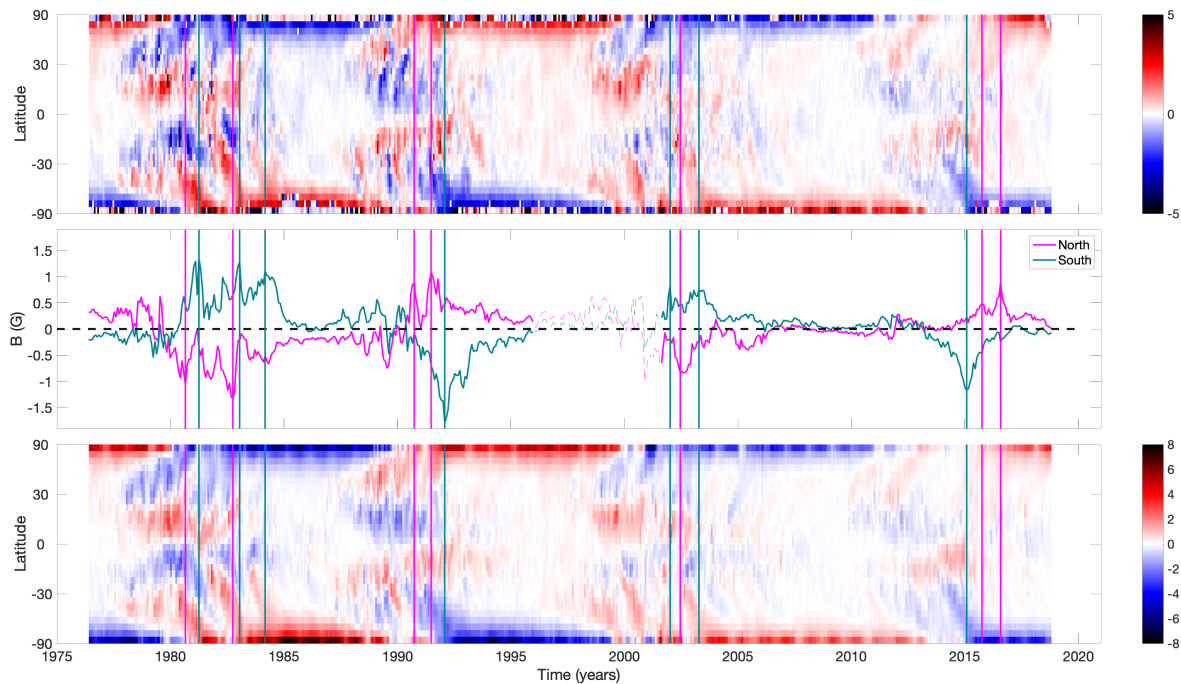


**Fig. 1.** Results for weak-field shifts from WSO synoptic maps. *Top:* weak-field shifts calculated for each latitude bin and rotation, called here the shift butterfly diagram (positive shifts in red, negative in blue). *Middle:* hemispheric shift values (north in pink, south in cyan). *Bottom:* longitudinal means of the photospheric field for each latitude bin and rotation, i.e., the normal magnetic butterfly diagram (positive field in red, negative in blue). Vertical lines denote the shift extrema (north in pink, south in cyan).

lower panel of Fig. 1 shows that the latitude span of the negative polarity in the northern hemisphere is very wide during the two extrema, especially during the latter extreme which gives the largest (negative) shift in the north in cycle 21.

The same correspondence between hemispheric shift extrema and surge evolution can be seen for the southern hemisphere during cycle 21, where we have identified three shift extrema. The corresponding surges of shifts and the magnetic field in the southern hemisphere are perhaps even more clearly visible than the surges in the northern hemisphere. For each of the three surges, the hemispheric shift maxima are located at times when the forward edge of the corresponding surge has recently reached the pole and the (positive) unipolar region of the surge extends from mid-latitudes until the pole. The bottom panel of Fig. 1 shows that the first positive surge turns the polar polarity for a year or so, but a subsequent surge of negative (leading) polarity interrupts this development. The effect of the negative-polarity surge is also seen as a sudden decrease of the hemispheric shift after its first extreme (see middle panel of Fig. 1). Still, at the same time the weak-field shift remains strong at the pole, as a consequence of the first surge. The new (positive) polarity of the southern pole is re-established by the second surge, during which the hemispheric shift attains its second extreme and the positive shifts in the southern hemisphere extend over a very wide range of latitudes. The third, slightly weaker surge in the south further strengthens the southern polar field and forms the third, slightly lower but longer maximum to the hemispheric shift.

It should be noted that the largest shift values around the southern pole are found soon after the third surge (polar shift values are partly missing due to poor data coverage). However, hemispheric (mean) shift reduces to a low value after the main surge activity has subsided and large shift values are only found around the pole. We also note how closely the weak-field shift

and the mean field follow each other at the two poles not only during the declining phase of solar cycle 21, but during the whole solar cycle and, in fact, during the whole data interval consisting of four solar cycles.

This connection of the hemispheric shifts to the surge evolution is seen perhaps most dramatically in the southern hemisphere during solar cycles 22 and 24 when, in both cycles, after a weaker prior surge, a very strong surge appeared and finally reversed the polarity of the southern pole. The middle panel of Fig. 1 shows in each of these two cases that this strong surge led to a sharp extreme in the southern shift soon after the forward edge of the surge reached the polar latitudes. At this time the southern unipolar (negative) field as well as the southern (negative) shift extended to quite low latitudes. Soon thereafter, well before the respective solar minima, surge activity subsided and the hemispheric mean shifts rapidly reduced to a rather low level, leaving large shift values only at the pole.

#### 4. SOLIS/VSM shifts

As we have shown earlier for rotational full-map shifts (see Figs. 3–6 and Table 1 in Getachew et al. 2019a) and for hemispheric shifts (see Figs. 1 and 2 and Table 1 in Getachew et al. 2019b), the value of the shift increases when decreasing the spatial resolution of the map. This change was found for all five of the different high-resolution datasets that we studied. This change is systematic, but not linear. The largest relative increase in the shift was found when the resolution was reduced to the supergranulation scale (Getachew et al. 2019a). Accordingly, we now study whether the surge pattern of shifts found in Fig. 1 for the extremely low-resolution WSO observations holds for other, higher resolution maps.

Figure 2 shows panels for SOLIS/VSM 1800\*900 pixel high-resolution maps similar to those depicted in Fig. 1 for

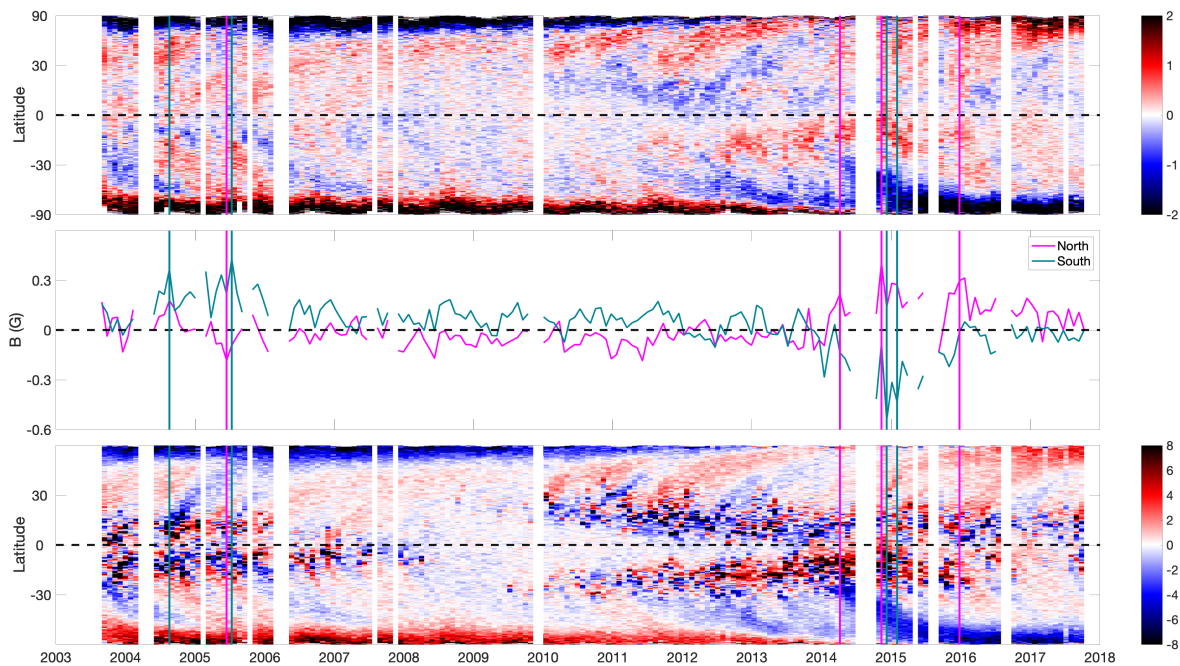


**Fig. 2.** Results for weak-field shifts from SOLIS/VSM synoptic maps. Panels are the same as in Fig. 1.

the low-resolution WSO maps. We note first the bottom panel (the normal butterfly diagram) of Fig. 2, which shows the magnetic evolution on the solar surface much more in detail than the corresponding WSO butterfly diagram in Fig. 1. The active regions and the surges are resolved in far better spatial resolution in Fig. 2 than in Fig. 1. Even so, the overall development of the large-scale magnetic fields, including poleward surges, remains very similar for the two datasets during the overlapping time.

The top panel of Fig. 2 shows that, even at this high spatial resolution, the weak-field shifts form shift surges similar to those in Fig. 1, evolving in close connection with the poleward surges of the background field. However, the shift surges in Fig. 2 are slightly less clear and less structured than the shift surges in Fig. 1 or the surges of the normal butterfly diagram in Fig. 2. This is due to the smaller absolute value of the (high-resolution) SOLIS shifts (as found in Getachew et al. 2019a), which increases the relative effect of noise in the top panel of Fig. 2 compared to Fig. 1. The overall scale of the (high-resolution) SOLIS shifts is indeed smaller than that for the (low-resolution) WSO shifts, in agreement with the increase in shifts with reducing spatial resolution. This is valid now even across the different instruments.

The hemispheric shifts of the SOLIS/VSM high-resolution maps (see middle panel of Fig. 2) show mostly weakly negative hemispheric shifts in the north until 2014 (mainly due to the negative polar shifts), whereafter they attain larger positive values until they decline again at the end of the time interval. Southern shifts attain large positive values at the start in 2004–2005, and remain weaker but mainly positive over the minimum until 2013, whereafter they attain large negative values around 2015 and then reduce to close to zero at the end. This long-term (solar cycle) evolution of the SOLIS hemispheric shifts is quite similar to that of WSO shifts during the overlapping time interval (cf. middle panels in Figs. 1 and 2). This further verifies the fact that the evolution of both the weaker shifts derived from the high-resolution SOLIS data and the larger low-resolution WSO

shifts is connected with the poleward surges that determine the cyclic evolution of the surface large-scale magnetic fields.

However, there are some systematic differences in the timing and the relative size of the extreme values of hemispheric shifts between SOLIS and WSO. The maximum of the southern SOLIS shift in the (admittedly, partially covered) cycle 23 occurs in mid-2005, and the level in 2003–2004 remains relatively lower than in WSO at the same time. In addition, the southern shift maximum in 2005 is much larger than the maximum (absolute) shift in the north, contrary to simultaneous WSO observations. During cycle 24, the extreme of the southern SOLIS shift at the turn of 2014–2015 coincides very well with the WSO shift extremum. However, the two first SOLIS shift extrema in the north in early and late 2014 (see middle panel of Fig. 2) are much higher with respect to the third peak in 2016 than the relative height of the two peaks for WSO shifts (see middle panel of Fig. 1, where only the latter two are seen and noted as extrema).

Because of the small data gaps in SOLIS synoptic maps and in Fig. 2 these considerations regarding the differences in the timing and relative height of the shift extrema between WSO and SOLIS might be thought to be not solid or significant. In order to further study these differences and to prove that not only are they valid, but also interesting and essential, we depict in Fig. 3 the SOLIS hemispheric shifts for four additional (lower) resolutions, obtained from the original data by block averaging (for more details, see Getachew et al. 2019a).

Figure 3 shows the similar long-term evolution of SOLIS shifts for all resolutions. However, even more interestingly, some systematic changes in the timing and height of SOLIS shift extrema when reducing the spatial resolution can be seen. For example, the weak northern (negative) extreme in 2005 becomes systematically larger in absolute value when reducing the spatial resolution of synoptic maps (five top left panels of Fig. 3). The three lowest resolution SOLIS shifts form an indisputed (local) extremum in 2005, in agreement with WSO observations (bottom left panel of Fig. 3). There is a better agreement between

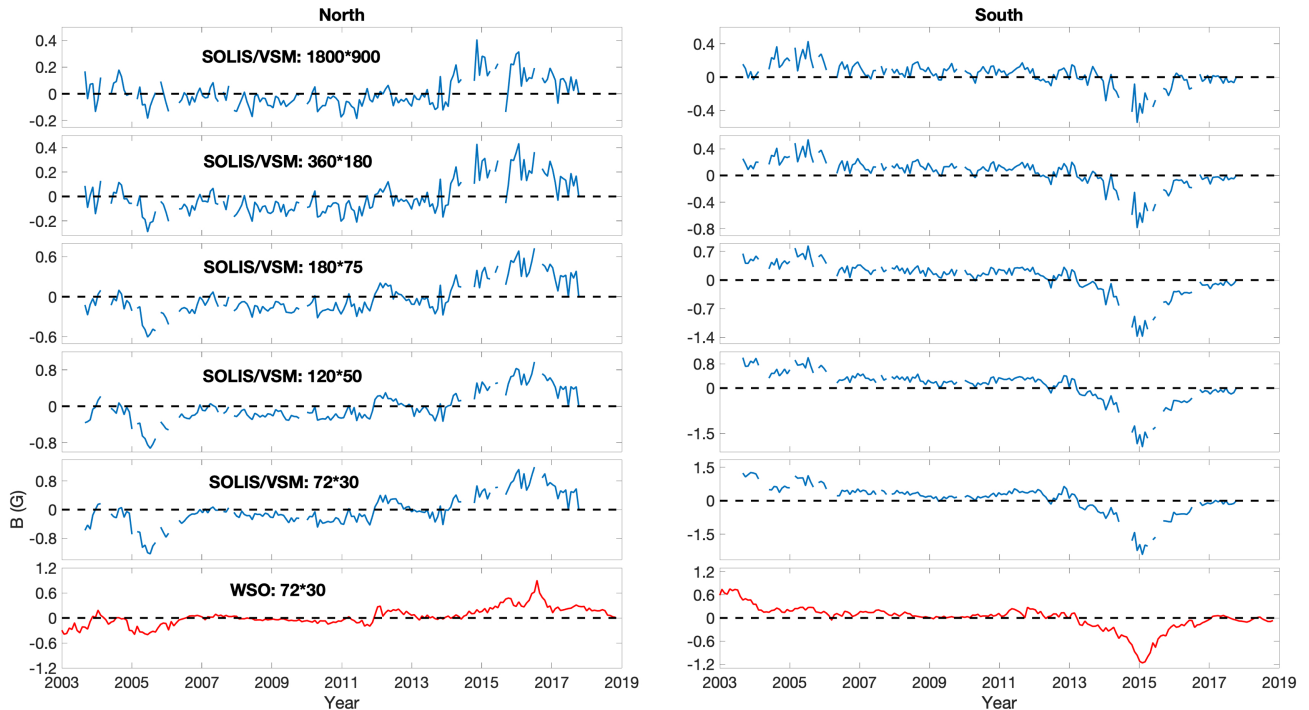


**Fig. 3.** Hemispheric weak-field shifts of SOLIS/VSM synoptic map for (from top to bottom) 1800\*900, 360\*180, 180\*75, 120\*50, and 72\*30 resolutions. *Left panels* are for the northern hemisphere and *right panels* for the southern hemisphere.

the SOLIS and WSO north shifts even before this extremum, at the start of SOLIS data interval, with the first SOLIS shift values becoming systematically more negative with reducing resolution. At the same time, in the south (see right panels of Fig. 3) the relative height of SOLIS shifts between 2003–2004 and 2005 is reversed when reducing the resolution from 1800\*900 to 72\*30. Similarly to the northern shifts, this change with spatial resolution makes the low-resolution shifts of SOLIS agree better with the WSO shifts than the high-resolution SOLIS shifts.

Perhaps the most dramatic changes related to reducing the SOLIS resolution in Fig. 3 are those related to the extrema of the northern hemisphere in 2014–2016. One can see a systematic relative decrease in the (positive) shifts in 2014 and in early 2015 and a systematic relative (and absolute) increase in shifts in 2016 (note the changing scale of the panels in Fig. 3). These changes move the highest shift maximum in the north from the high-resolution peak in 2014 to the low-resolution peak in 2016, whereafter the low-resolution extrema in 2016 in SOLIS and WSO agree very well with each other (despite the small data gap in 2016). We also note that there is a similar but much smaller change in the timing of the shift extremum in the southern hemisphere from late 2014 for the high-resolution SOLIS maps to early 2015 for the low-resolution maps. The latter timing agrees perfectly with the timing of WSO shift extreme.

The largest quantitative and even qualitative changes in Fig. 3 take place when changing from 360\*180 pixel resolution to 180\*75 resolution. The absolute levels of shift extrema increase by about 50% from 1800\*900 to 360\*180 pixels (increase in spatial scale by a factor of 25), but become almost two times larger in a much smaller transition from 360\*180 to 180\*75 pixels (increase by a factor of 4.8). The subsequent increase is also smaller, only about 50%, from 180\*75 to 72\*30 pixels (increase by a factor of 6.25). The average size of supergranulation diameter is about  $2.4^\circ$  or 30 000 km (for a

review, see, e.g., Rincon & Rieutord 2018), which is very close to the 180\*75 pixel resolution of synoptic maps.

The specific nature of the change of SOLIS resolution from 360\*180 to 180\*75 pixels is seen not only in the increase of absolute levels but also in the change of relative levels between the SOLIS maps of different resolutions. This is seen, for example, in the north in the lowering of the relatively higher shift levels in 2014–2015 in the two highest resolution maps (the two top left panels in Fig. 3) to relatively lower shift values compared to shift values in 2016, setting the 2014–2015 shift values in the high-resolution maps clearly below the 2016 shift levels in all lower resolution maps. In the south, an increase in the shift level in 2003 above the level in 2004 is also seen when lowering the SOLIS resolution from 360\*180 pixels to 180\*75 pixels. These results give strong additional evidence for the idea that both quantitative and qualitative changes take place in the weak-field shifts at the supergranular scale (Getachew et al. 2019a).

We note that supergranular diffusion is an essential element, for example, in surface flux transport models (Sheeley et al. 1987; Wang et al. 1989; Mackay & Yeates 2012; Virtanen et al. 2017) that aim to describe the spatial-temporal evolution of the main magnetic field. Supergranular diffusion contributes to the meridional transport of magnetic flux, and therefore to the formation and properties of surges and to the development of unipolar fields at the poles. Diffusion proceeds over a wide range of scales, but the physical character of diffusion (e.g., level of diffusion and its spectral index) seems to depend on the scale studied and the way (parameter) diffusion is measured. However, a number of recent studies have found that there may be a transition in the properties of diffusion across the supergranulation scale (Iida 2016; Abramenko 2017; Skokić et al. 2019), which would support our finding of the enhanced scale dependence of the weak-field shift at the supergranulation scale.

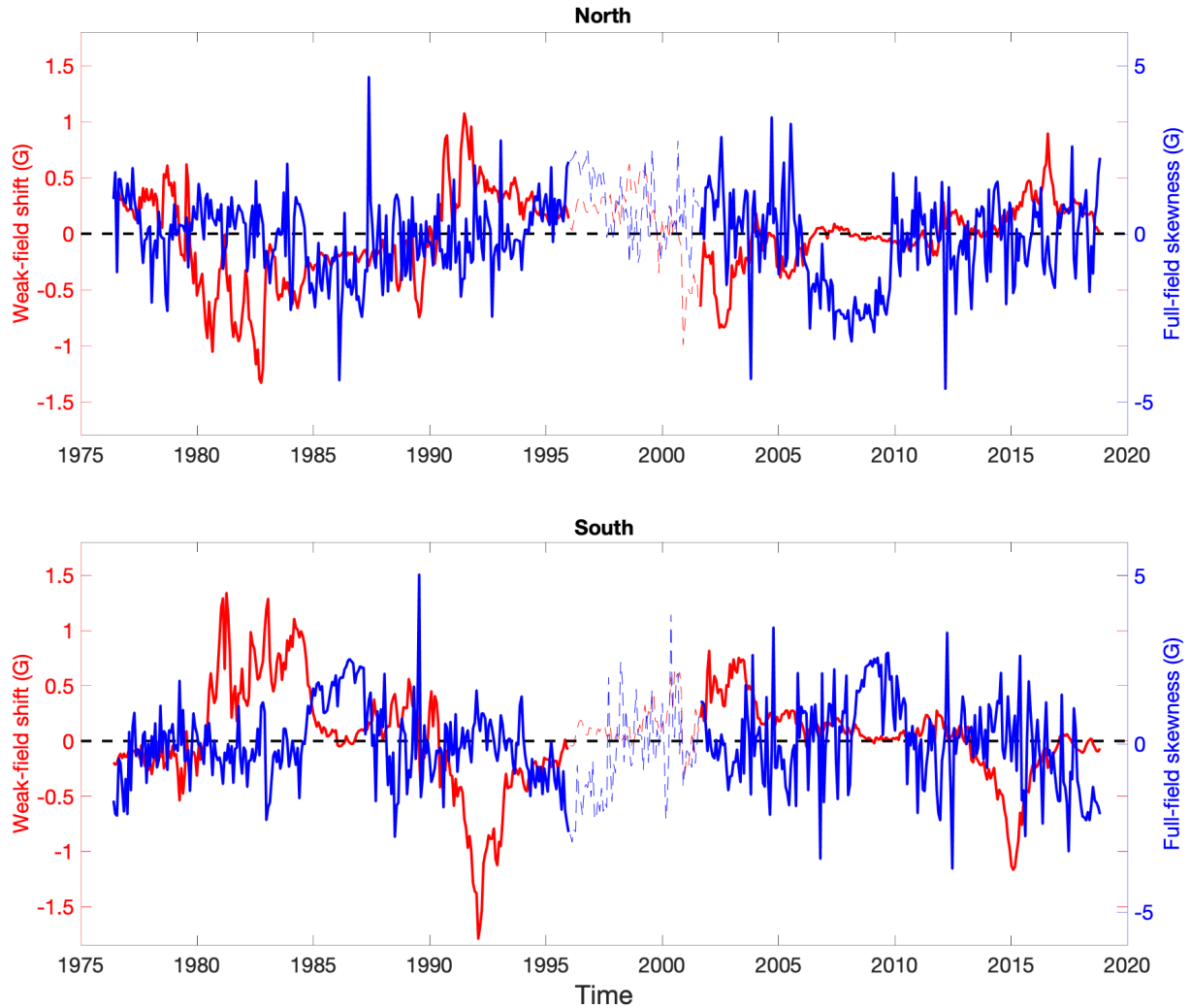


**Fig. 4.** Hemispheric weak-field shifts (red; *left* y-axis scale) and full-field skewnesses (blue; *right* y-axis scale) for each WSO synoptic map.

## 5. Skewness

Skewness, the third moment of the distribution function, is a measure of the asymmetry of the data set around its mean. Skewness is positive if the data points are spread out more to the positive side of the mean than to the negative side, and vice versa for negative skewness. Figure 4 depicts the hemispheric weak-field shifts (copied from the middle panel of Fig. 1) and the hemispheric skewness for all field values of the WSO synoptic maps (to be called here the full-field skewness). Figure 4 shows that the hemispheric means of WSO full-field skewness are mostly zero, but attain systematically non-zero values around sunspot minima. Full-field skewness in the north is negative during the negative polarity minima after the mid-1980s and in the late 2000s, and positive around positive polarity minimum in the mid-1990s, although most of related data are incorrect. The values in the late 2010s are not yet systematically positive. Similarly, the southern full-field skewness attains systematically positive values after the mid-1980s and in the late 2000s and negative values after the mid-1990s and in the late 2010s (where systematically negative values already appear).

Figure 5 depicts the full-field skewness butterfly diagram for SOLIS synoptic maps of highest resolution (top panel) and a similar butterfly diagram using only weak field values limited to the same range (from  $-10$  G to  $+10$  G; weak-field skewness;

middle panel) as the weak-field shift, together with the normal magnetic butterfly diagram (bottom panel). The top panel shows that the full-field skewness has a spatial–temporal evolution similar to the normal magnetic butterfly diagram (and the weak-field shift). The full-field skewness depicts the same dominant surges with the same sign (polarity), as well as the unipolar polar values as the normal magnetic butterfly diagram. This shows that the distribution of all magnetic field values (especially the large values; see below) is systematically skewed toward the dominant polarity. This pattern is true since the emergence of active regions up to and including the accumulation of unipolar fields at the poles. We also note that the SOLIS full-field skewness depicts a strong annual variation at high to polar latitudes due to the Earth’s varying heliographic latitude (so called vantage point or  $b_0$ -angle effect; for a recent discussion, see Virtanen & Mursula 2017). Annual maxima of skewness are found in fall (spring) for the northern (southern) hemisphere when the Earth is at its highest northern (southern) heliographic latitude, and the unipolar regions around the north (south) pole can be better viewed.

A similar vantage point related annual variation can also be seen at high latitudes of the normal magnetic butterfly diagram, especially clearly in the case of (the low-resolution) WSO observations (see bottom panel of Fig. 1), but less strongly even in the (high-resolution) SOLIS butterfly diagram (see bottom panel

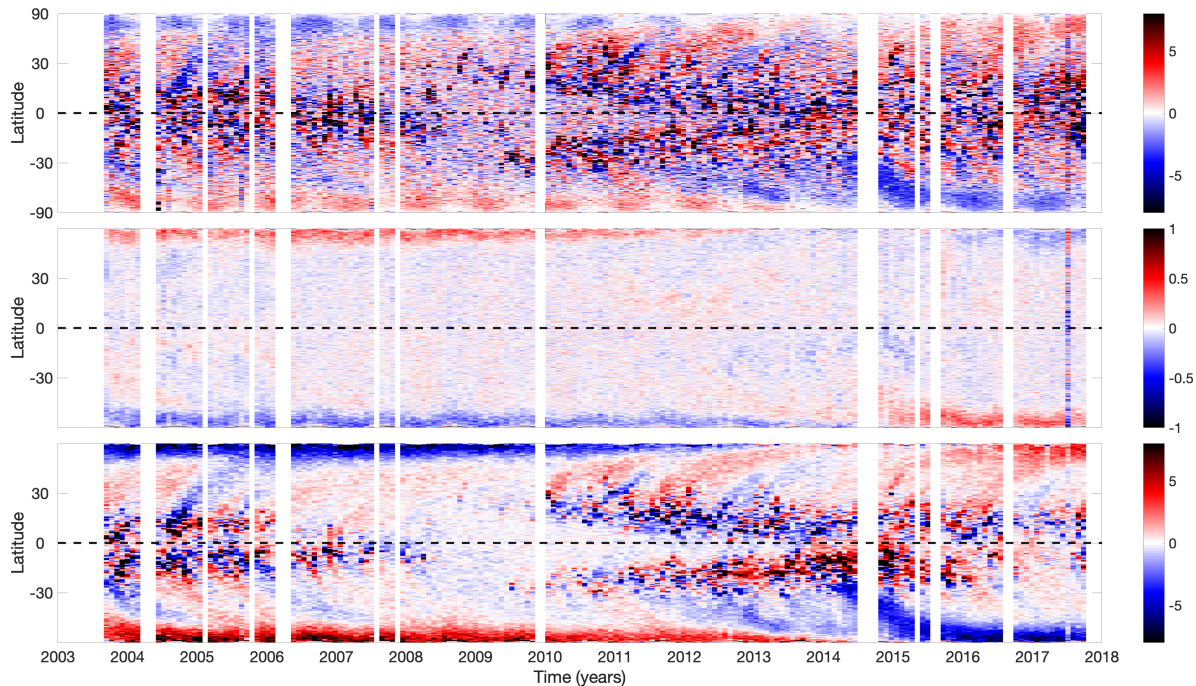


**Fig. 5.** Results for skewness from SOLIS/VSM synoptic maps. *Top*: skewness calculated for each latitude bin and rotation using all field values, called here the full-field skewness butterfly diagram (positive skewness in red, negative in blue). *Middle*: same as in top panel, but using only weak-field values to calculate skewness, called here the weak-field skewness butterfly diagram. *Bottom*: longitudinal means of the photospheric field for each latitude bin and rotation, known as the normal magnetic butterfly diagram.

of Fig. 2). This annual variation attains its maximum around solar minima when the latitudinal gradient of the magnetic field between the non-zero pole and the weaker mean field at a somewhat lower latitude is largest. It should also be noted that the relative amplitude of the annual variation is larger for skewness than for the main field since larger values of the field, which are more important for skewness, are more vulnerable to being suppressed by weaker visibility.

The middle panel of Fig. 5 depicts the SOLIS high-resolution weak-field skewness. The pattern of the weak-field skewness butterfly diagram is very different from the corresponding full-field diagram. First of all, the range of weak-field skewness values is almost an order of magnitude smaller than for the full-field skewness. Since skewness weights the difference to the mean by the third power, this difference is easily understandable. Large field values have the strongest weight in skewness, making the full-field skewness larger. Secondly, the weak-field skewness has very weak values (close to zero) at most latitudes at all times, and systematically non-zero values only at polar latitudes. Third, and perhaps surprisingly, the sign (polarity) of the weak-field skewness at the poles is opposite to that of the full-field polar skewness.

We show this seeming contradiction in Fig. 6, which gives a sample distribution of SOLIS high-resolution field values at high southern latitudes (poleward of  $-70^\circ$ ) for CR 2052 (January 2007), together with the Gaussian fit to weak field values that was used to determine the weak-field shift. Figure 6 shows that the maxima of the distribution and of the Gaussian fit to the weak field values (the weak-field shift) are shifted to positive values. The weak-field shift in the southern pole at this time is about 3 G, i.e., more than an order of magnitude larger than the hemispheric mean shift (see middle panel of Fig. 2).

Interestingly, the distribution of Fig. 6 is asymmetric in two ways. Around the peak, the distribution is skewed toward zero,

i.e., it has more values on the negative side of the distribution than on the positive side. This means that the weak-field skewness is negative at this time, as depicted in the middle panel of Fig. 5. On the other hand, at larger field values (above about 10–15 G) the distribution is skewed toward positive values. These larger field values yield the positive skewness of all field values (the full-field skewness), as seen in the top panel of Fig. 5. We note that the pattern of Fig. 6 remains the same in the south for many years, and that the pattern in the north is a mirror-image of that depicted in Fig. 6. This explains the seeming contradiction between the two skewness butterflies.

## 6. Discussion

We studied here the spatial–temporal evolution of (non-zero) shifts of weak photospheric magnetic field values using WSO and SOLIS/VSM synoptic maps. Shifts were calculated by fitting the histogram distribution of weak-field values (here within  $\pm 10$  G) of the respective part of each synoptic map to a shifted Gaussian, as presented in detail in Getachew et al. (2019a). We also examined the spatial–temporal evolution of the skewness of the distribution of all field values and, separately, the skewness of the distribution of weak field values ( $\pm 10$  G).

We found that the spatial–temporal evolution of weak-field shifts is closely related to the appearance of active regions and the subsequent poleward drift of the largest surges of (mainly) trailing polarity magnetic fields, and thereby closely follows the solar cycle evolution of large-scale magnetic fields on the solar surface. Observations even at the highest spatial resolution of SOLIS/VSM maps show that the maximum of the weak-field distribution is slightly but systematically shifted towards the dominant polarity of the surge already at the appearance of the active region. During the surge evolution the high-resolution shifts can attain somewhat different values, but

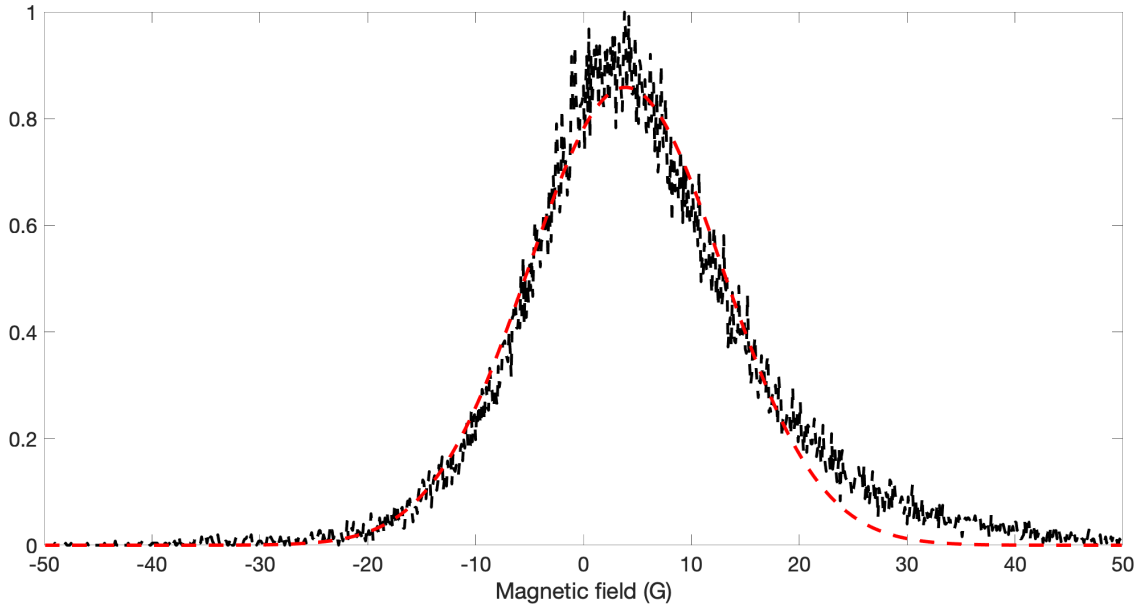


**Fig. 6.** Distribution of SOLIS high-resolution field values at high southern latitudes (poleward of  $-70^\circ$ ) for CR 2052 (January 2007; black dashed line), together with the Gaussian fit to weak field values (red dashed line).

typical shift values remain at a roughly similar, quite low mean level (below 0.5 G). However, during a few very strong surges, as in 2014–2015 in the south and 2016–2017 in the north, there is evidence that the high-resolution shift values become slightly stronger during the surge evolution.

Interestingly, the high-resolution shift values at the poles are found to be considerably larger (typically a few gauss) than during the surge evolution. The polar high-resolution shifts also remain at a high level for several years, throughout the declining phase and the subsequent minimum, reducing only during the ensuing ascending phase (see Fig. 2). This evolution recalls the evolution of polar fields, where unipolar flux is transported to the poles by the surges. However, the shift does not grow if elements of magnetic field with the same distribution (and shift) are joined together. This gives strong evidence for the cancellation of opposite-polarity fields at the (not completely unipolar) poles to produce more of weak-field values with the dominant polarity. This process continues as long as there is a sufficient density of opposite-polarity elements, and leads to a slow weakening of the polar shifts during several years.

The weak-field shifts calculated from the lower-resolution data (WSO and lowered-resolution SOLIS data) are larger (about 1 G) than the high-resolution shifts during the whole surge evolution. This is due to the fact that, at a lower resolution, the data effectively adds together (higher resolution) elements of stronger flux with opposite polarity to increase the pre-existing (higher resolution) weak-field shift. We have found evidence that the low-resolution weak-field shifts grow during surge evolution. Moreover, this increase in low-resolution weak-field shifts during surge evolution seems to be most effective when the reduction of resolution approaches the supergranulation scale. This gives evidence that the above-mentioned coalescence of opposite-polarity fields also proceeds during the surge evolution, and is most effective at a rather low resolution, at and lower than the supergranulation scale.

However, more interestingly, while the low-resolution shifts are larger than high-resolution shifts during the surges, they do not increase from surge to pole by such a large factor as the

high-resolution shifts. Moreover, the low-resolution polar shifts have roughly the same value as the high-resolution shifts. Taking into account the effective coalescence of opposite-polarity fields that increases polar high-resolution shifts, the same should take place also, at least as effectively, for the low-resolution shifts. Since this does not take place, this suggests that there is no spatial structure in the unipolar polar regions that would greatly increase polar low-resolution shifts. Accordingly, our results suggest a lack or significant weakening of the supergranulation process at the solar poles.

We also studied here skewness, the statistical parameter that quantifies the possible asymmetric (skewed) shape of a distribution. While the shift is heavily weighted by those weak field values that have the largest numbers (peak of distribution), skewness is much more strongly weighted by field values that are farther away from the mean. We found that the skewness calculated using all SOLIS high-resolution field values (full-field skewness) followed closely the same spatial–temporal evolution as the weak-field shifts and the large-scale photospheric magnetic field. During the surges and around the poles, the full-field skewness was found to have a sign that indicates that the distribution of moderate and large field values has a preference toward the dominant polarity in the area.

Figure 5 (top panel) shows that the full-field skewness attains its largest values already at the flux emergence, not during the later phase of surge evolution or at the poles. The polar values of full-field skewness are not larger than those during the surge, contrary in particular to the high-resolution weak-field shifts. This evolution of skewness during surge evolution and at the poles can be understood to result from the coalescence of larger fields of opposite polarity, which reduces skewness (and increases weak-field shift). We also note how closely the polar full-field skewness and polar weak-field shifts (top panels of Figs. 2 and 5, respectively) follow each other over the solar cycle, with skewness weakening to zero slightly before the shift.

We also studied the skewness of the weak field values (within  $\pm 10$  G), and found that the weak-field skewness is very weak (practically zero) everywhere except for the polar region during

the declining and minimum phases of the solar cycle. We showed that the distribution of polar weak-field values is skewed toward zero (weaker absolute values). Accordingly, the polar weak-field skewness always has an opposite sign (polarity) to the weak-field shift and to the prevailing field polarity. This gives further evidence for the coalescence of opposite-polarity fields, which not only increases the field values around the distribution maximum, thus increasing the weak-field shift, but also increases those very weak field values that are even smaller than the absolute value of the shift.

## 7. Conclusions

In conclusion, after studying the long-term evolution of weak photospheric magnetic field values at different spatial resolutions we find the following results:

- There is evidence for a systematic non-zero weak-field shift and skewness of the field distribution already at (and after) the emergence of the active region.
- Weak-field shifts and full-field skewness depict a spatial-temporal solar cycle evolution very similar to the large-scale surface magnetic field.
- We find evidence for a continuing coalescence of opposite-polarity fields during the surge evolution and at the poles, which increases the weak-field shift. During surge evolution, coalescence was found to be more effective at low spatial resolution, roughly at the supergranulation scale.
- A similar dependence on spatial resolution was not found in the unipolar regions around the poles. Instead, high-resolution and low-resolution shifts attained quite similar large values at the poles. This suggests that the supergranulation process is considerably reduced or turned off in the unipolar regions around the poles. Reduced supergranulation at polar latitudes may be the physical reason to determine the equatorial boundary, and thus the size of the polar area. These conclusions need to be further verified by additional evidence using more direct observations of supergranulation. These observations improve the understanding not only of the development of the weakest magnetic field elements, but also of

the dynamics of magnetic fields at large, and even of processes below the solar surface.

*Acknowledgements.* We acknowledge the financial support by the Academy of Finland to the ReSoLVE Centre of Excellence (project no. 307411). Wilcox Solar Observatory data used in this study was obtained via the website <http://wso.stanford.edu> courtesy of J. T. Hoeksema. Data were acquired by SOLIS instruments operated by NISP/NSO/AURA/NSF.

## References

- Abramenko, V. I. 2017, *MNRAS*, **471**, 3871  
 Babcock, H. W. 1961, *ApJ*, **133**, 572  
 Berger, T., & Lites, B. 2002, *Sol. Phys.*, **208**, 181  
 Berger, T., & Lites, B. 2003, *Sol. Phys.*, **213**, 213  
 Bertello, L., Pevtsov, A. A., Petrie, G. J. D., & Keys, D. 2014, *Sol. Phys.*, **289**, 2419  
 Getachew, T., Virtanen, I., & Mursula, K. 2019a, *ApJ*, **874**, 116  
 Getachew, T., Virtanen, I., & Mursula, K. 2019b, *Geophys. Res. Lett.*, **46**, 9327  
 Hagenaar, H. J., Schrijver, C. J., & Title, A. M. 2003, *ApJ*, **584**, 1107  
 Hagenaar, H. J., DeRosa, M. L., & Schrijver, C. J. 2008, *ApJ*, **678**, 541  
 Hale, G. E., Ellerman, F., Nicholson, S. B., & Joy, A. H. 1919, *ApJ*, **49**, 153  
 Hoeksema, J. T. 1984, PhD Thesis, Stanford University  
 Iida, Y. 2016, *J. Space Weather Space Clim.*, **6**, A27  
 Leighton, R. B. 1969, *ApJ*, **156**, 1  
 Lites, B. W. 2002, *ApJ*, **573**, 431  
 Liu, Y., Zhao, X., & Hoeksema, J. T. 2004, *Sol. Phys.*, **219**, 39  
 Mackay, D. H., & Yeates, A. R. 2012, *Liv. Rev. Sol. Phys.*, **9**, 6  
 Okamoto, T. J., & Sakurai, T. 2018, *ApJ*, **852**, L16  
 Rincon, F., & Rieutord, M. 2018, *Liv. Rev. Sol. Phys.*, **15**, 6  
 Sheeley, N. R., Jr., Nash, A. G., & Wang, Y. M. 1987, *ApJ*, **319**, 481  
 Skokić, I., Brajša, R., Sudar, D., Ruždjak, D., & Saar, S. H. 2019, *ApJ*, **877**, 142  
 Stenflo, J. O. 1989, *A&ARv*, **1**, 3  
 Stenflo, J. O. 2010, *A&A*, **517**, A37  
 Stenflo, J. O. 2014, in *Solar Polarization 7*, eds. K. N. Nagendra, J. O. Stenflo, Q. Qu, & M. Samooprna, *ASP Conf. Ser.*, **489**, 3  
 Stenflo, J. O. 2017, *Space Sci. Rev.*, **210**, 5  
 Tlatov, A. G., Vasil'eva, V. V., & Pevtsov, A. A. 2010, *ApJ*, **717**, 357  
 Ulrich, R. K., Evans, S., Boyden, J. E., & Webster, L. 2002, *ApJS*, **139**, 259  
 van Driel-Gesztelyi, L., & Green, L. M. 2015, *Liv. Rev. Sol. Phys.*, **12**, 1  
 Virtanen, I., & Mursula, K. 2016, *A&A*, **591**, A78  
 Virtanen, I., & Mursula, K. 2017, *A&A*, **604**, A7  
 Virtanen, I. O. I., Virtanen, I. I., Pevtsov, A. A., Yeates, A., & Mursula, K. 2017, *A&A*, **604**, A8  
 Wang, Y. M., Nash, A. G., & Sheeley, N. R., Jr. 1989, *Science*, **245**, 712  
 Zirin, H. 1987, *Sol. Phys.*, **110**, 101